Proceedings of the 2009 IEEE International Conference on Systems, Man, and Cybernetics
San Antonio, TX, USA - October 2009

A control strategy for steering an autonomous surface sailing vehicle in a tacking maneuver

Jerome Jouffroy
Mads Clausen Institute
University of Southern Denmark (SDU)
Alsion 2, DK-6400 Sønderborg, Denmark
e-mail: jerome@mci.sdu.dk

***Abstract*— Sailing vessels such as sailboats but also landyachts are vehicles representing a real challenge for automation. However, the control aspects of such vehicles were hitherto very little studied. This paper presents a simplified dynamic model of a so-called landyacht allowing to capture the main elements of the behavior of surface sailing vessels. We then propose a path generation scheme and a controller design for a well-known and fundamental maneuver in sailing referred to as tacking. Simulation results are presented to illustrate the approach.**

I. Introduction

Whether they are aerial, marine, submarine or road vehicles, autonomous vehicles are experimental platforms still widely used in different aspects of control research, such as motion planning, feedback, or formation control. Surprisingly, there is comparatively very little research on vehicles using a flow present in the environment as their main means of propulsion. Among these vehicles, one can obviously think of the well-known sailboats, but other vehicles, also evolving on a surface, such as kite-buggies or landyachts, share the same basic dynamic properties of sailing vessels. Most studies on these vehicles, such as [13], consider Artificial Intelligence-based techniques for the control strategies and do not make use of the available dynamic models that would allow for further analysis to assess for example stability or performance. Another reference, [12], adopts a more traditional model-based perspective, but its control design is solely based on a linear model structure, thus not allowing for the study of dynamical aspects and maneuvers that are specific to sailing vehicles, such as tacking, jibing or wearing.

In sailing, one of the main concerns for the navigator is to plan maneuvers toward a given destination, taking into account these specificities. When considering autonomous vehicles, another interest is to compute or plan the signals necessary to steer the vehicle on the desired paths. In many areas concerned with motion control, such as mobile robotics or marine control, this is usually done by guidance systems and trajectory generation, whose role is mostly to plan and compute desired trajectories that are feasible for the autonomous vehicle (see for example [6] for car-like robots, but also [2, chapter 5] in marine control).

In this paper, we propose to model and study control aspects related to motion planning issues of a landyacht. A landyacht is basically composed of a cart with three wheels and a sail (see picture of our experimental platform Mad Mads 1 in Figure 1). This vehicle is controlled by changing the angle of the front wheel through pedals for steering, and a simple rope attached to the sail for propulsion. After this introduction, section 2 will be dedicated to formalize a simple model of a landyacht. Like in mobile robotics, our model is based on a basic kinematic structure, albeit completed with a simple dynamic equation to account for the specificities of the system responsible for propulsion. Incidentally, other types of surface sailing vessels share similar characteristics. The following section is dedicated to path generation and controller design for an important maneuver in sailing: tacking. Of particular interest is a dynamic-related condition for performing a tack maneuver, condition that is also related to common practise in sailing. Simulations results are presented to illustrate effects linked with this condition and the behavior of the proposed schemes. Finally, a few concluding remarks end the paper.

Fig. 1. Picture of Mad Mads 1 from SDU.

II. Modeling of a landyacht

In order to study motion planning issues for our sailing vehicle, but also to gain insight on the problem at hand, we would like to have at our disposal a simple way to represent dynamically the relatively complex maneuvers that

978-1-4244-2794-9/09/$25.00 ©2009 IEEE

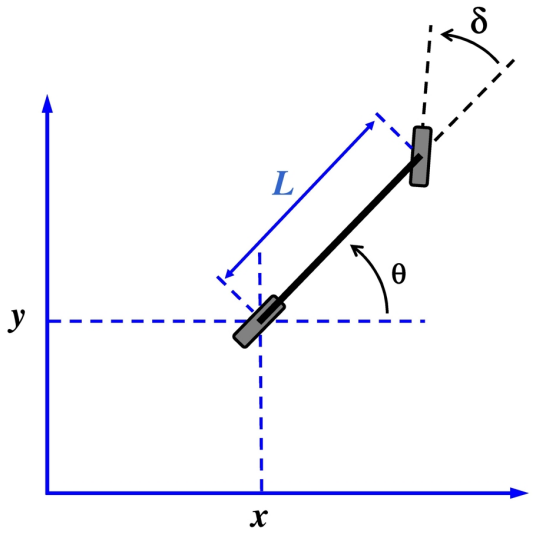

Fig. 2. The Dubins car model

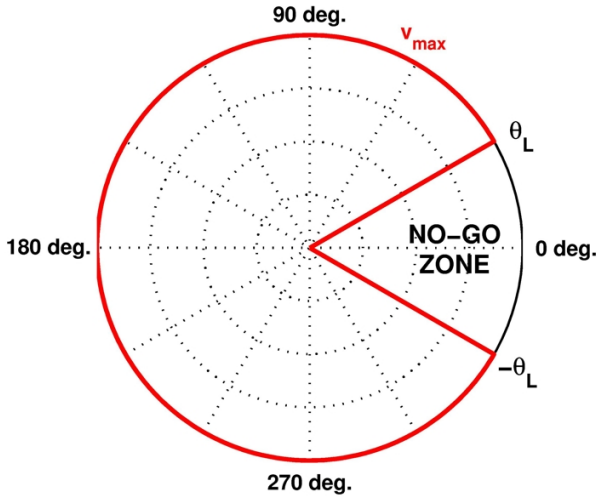

Fig. 3. Polar curve of the propulsive system

such vehicles can perform. To this end, first consider that our landyacht is nothing but, roughly speaking, a car whose propulsive part is a sail.

Hence, owing to the vast literature on the subject in mobile robotics (see for example [6][7][9][5]), introduce first the well-known kinematic car model, also called bicycle model or Dubins car, represented in Figure 2, where the front wheel is steering the vehicle, while the rear center wheel is an approximation of the motion induced by the two rear wheels of the cart.

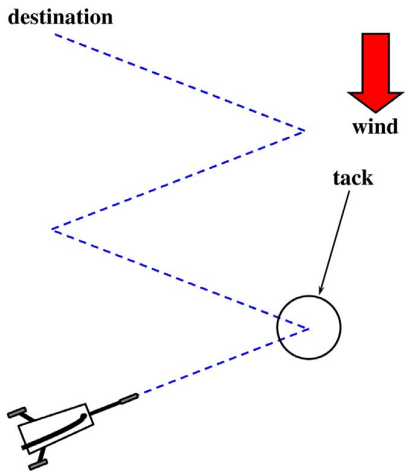

Fig. 4. Tacking maneuvers to go upwind

The kinematic model of the Dubins car is

$$\dot{x}(t) = v(t)\cos\theta(t) \quad (1)$$

$$\dot{y}(t) = v(t)\sin\theta(t) \quad (2)$$

$$\dot{\theta}(t) = \frac{v(t)}{L}\tan\delta(t) \quad (3)$$

where x, y represent the position of the contact point between the rear wheel and the ground, and θ its heading. The steering angle δ is normally directly controlled by the pilot and is henceforth considered as a control input. Parameter L is the distance between the two wheel axes (see Figure 2). In a usual Dubins car model, the longitudinal velocity $v(t)$ of the rear wheel axis is considered as a control input, either directly, or through an integrator (see [7]).

However, because of the specificities of our propulsion system, i.e. a sail, the velocities $v(t)$ that a vehicle can reach mostly depend on its orientation with respect to the wind. Indeed, and as is well-known by sailors, if the vehicle is too close to facing the wind, it will loose propulsion. This is illustrated by the so-called "no-sailing zone" or "no-go zone", as represented in Figure 3, assuming a wind coming from the east.

Despite this limitation, a sailing vehicle can reach a destination upwind by zigzagging in the direction of the wind, i.e. by staying out of the no-go zone on long transients alternated by short crossings of the no-go zone, called "tacks" (see Figure 4). To be able for the vehicle to perform a tack also indicates the presence of some intertia effect on the velocity $v(t)$. Thus, to model this fundamental behavior in sailing, we propose the following equation.

$$m\dot{v}(t) + dv(t) = d.\rho(\theta(t), v_s(t)) \quad (4)$$

where m and d play the role of a mass and a damping coefficient to account for the global dynamics of the vehicle in a tack. Function $\rho(\theta(t), v_s(t))$ plays the role of a performance

polar diagram in sailing by giving the maximum reachable velocity of the vehicle depending both on its orientation $\theta(t)$ and on the way the propulsion system is trimmed, represented by the control input $v_s(t)$.

Although $\rho(\theta(t), v_s(t))$ can take many complex shapes depending on the characteristics of the sailing vehicle (see for example [8][10]), we will in the following assume that it is defined as

$$p(\theta(t), v_s(t)) = \begin{cases} 0 & \text{if } |\theta(t)| \leq \theta_L \\ sat_{v_{\max}}(v_s(t)) & \text{otherwise} \end{cases} \quad (5)$$

and constructed after the limits θ_L and $-\theta_L$ of the no-sailing zone, since we are mostly interested in the role of this dead zone in our model. $v_{\max}$ is the maximum velocity that the vehicle can reach and is related to wind speed. In the following, we assume $v_{\max}$ to be constant.

Interestingly, the simple dynamical model (1)-(4) raises important questions regarding controllability properties that can generally be related to the behavior of sailing vehicles. Indeed, performing a tack efficiently is important if one wants not to lose too much speed while crossing the no-go zone, or worse to get stuck there. In the particular case of a landyacht, it is especially relevant, because after it is in irons, there is sometimes no other way to restart than for the pilot to push his vehicle. This is clearly not suitable for an autonomous vehicle.

To see the essential role played by the no-go zone in our model, first consider the vehicle as it just enters the no-go zone, with a heading of either $\theta(t) = \theta_L$ or $\theta(t) = -\theta_L$. In this situation, (4) reduces to

$$m\dot{v}(t) + dv(t) = 0 \quad (6)$$

with an initial velocity v_0. Integration obviously gives

$$v(t) = v_0 e^{-\frac{d}{m}t} \quad (7)$$

Because of the structure of model (1)-(3), integrating in turn $v(t)$ gives

$$\int_0^t v(\tau)d\tau = \int_0^t \sqrt{\dot{x}^2(\tau) + \dot{y}^2(\tau)}d\tau := l(t) \quad (8)$$

which corresponds to the arclength of the path followed by the vehicle. If the vehicle stays in the no-sailing zone, then the arclength will be (using (7))

$$l(t) = v_0 \left(-\frac{m}{d}e^{-\frac{d}{m}t} + \frac{m}{d}\right) \quad (9)$$

which, to the limit, gives

$$l_\infty := \lim_{t_2 \to \infty} l(t) = v_0 \frac{m}{d} \quad (10)$$

This in turn means that l_∞ is the maximum distance the vehicle can travel without catching the wind. In other words, in a tacking situation, it should reach the other side of the no-go zone in a shorter distance than l_∞ not to get stuck (or to be "in irons" as is usually said in the sailing word). This basically means making sharper turns. However, because the steering angle $\delta(t)$ is typically constrained to lie within a sector $[-\delta_L, \delta_L]$, where $0 < \delta_L < \pi/2$, there is also a limit in how sharp a turn can be, which in turn induces a limit on how short a path in the no-go zone can be. Clearly then, if the initial velocity v_0 is not sufficient, l_∞ could be lesser than the length of the path required to cross the no-go zone.

In terms of controllability notions (see [11] for a very good overview), this implies that there are situations where the point $\mathbf{x}_0 = (x_0, y_0, \theta_0 < -\theta_L, v_0)$ in the state-space cannot be controlled to $\mathbf{x}_T = (x_T, y_T, \theta_T > \theta_L, v_T)$ since no control input signals $v_s(t)$ and $\delta(t)$ exist for that purpose. Thus, the above simple observations imply that system (1)-(4) is not completely controllable.

III. Motion planning for a tacking maneuver

Even though they are dynamically coupled through model (1)-(4), the effects of the control inputs $v_s(t)$ and $\delta(t)$ are expected to be roughly separated as propulsion and steering, respectively. Assuming that the vehicle is to follow a pre-defined path, the steering will mostly depend on the position of the vehicle along the path. Hence, it will in the following be assumed that $v_s(t) = v_{\max}$, i.e. the sail is trimmed so that the maximum speed can be made out of the wind.

Defining a path in the plane by $x(\sigma)$, $y(\sigma)$, where $\sigma(t)$ is a scalar parametrizing the path, equation (1)-(3) can be simply transformed into

$$\frac{dx}{d\sigma}(\sigma(t))\dot{\sigma}(t) = v(t)\cos\theta(\sigma(t)) \quad (11)$$

$$\frac{dy}{d\sigma}(\sigma(t))\dot{\sigma}(t) = v(t)\sin\theta(\sigma(t)) \quad (12)$$

$$\frac{d\theta}{d\sigma}(\sigma(t))\dot{\sigma}(t) = \frac{v(t)}{L}\tan\delta(t) \quad (13)$$

where $\theta(\sigma)$ is defined from $\tan\theta(\sigma) = (dy/d\sigma)/(dx/d\sigma)$. Then, isolating $\delta(t)$ in (13) gives

$$\delta(t) = \arctan\left(\frac{L}{v(t)}\frac{d\theta}{d\sigma}(\sigma(t))\dot{\sigma}(t)\right) \quad (14)$$

Squaring then (11) and (12), one obtains

$$\dot{\sigma}(t) = v(t)\frac{1}{\sqrt{\left(\frac{dx}{d\sigma}(\sigma(t))\right)^2 + \left(\frac{dy}{d\sigma}(\sigma(t))\right)^2}} \quad (15)$$

Finally, using (15) in (14) gives

$$\delta(t) = \arctan\left(L\frac{d\theta}{d\sigma}(\sigma(t))\left[\left(\frac{dx}{d\sigma}(\sigma(t))\right)^2 + \left(\frac{dy}{d\sigma}(\sigma(t))\right)^2\right]^{-\frac{1}{2}}\right) \quad (16)$$

i.e. the steering angle is a function of the position of the vehicle on the path, represented by the path variable σ. As expected, the evolution of the latter is essentially determined by the velocity of the vehicle $v(t)$ through equation (15) (we assume that $\sigma(0) = 0$). Hence, equation (15) and (16) represent a feedforward controller for the steering angle of the vehicle.

In order to implement a path for a tacking maneuver, we will in the following use of combination of two clothoid arcs and two straight lines, as pictured in Figure 5. Clothoid arcs

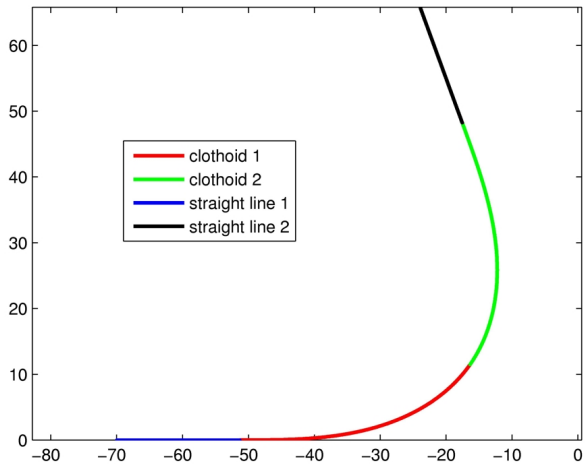

Fig. 5. Tacking maneuver path composed of two straight line segments and two clothoid arcs.

present the advantage of having zero curvature at their starting point, this ensuring a continuous transition with a straight line segment.

A clothoid is a curve whose tangent vector is a quadratic function of the path parameter σ, i.e.

$$\theta(\sigma) = \frac{k}{2}\sigma^2 + \kappa_0\sigma + \theta(0) \tag{17}$$

where k is a shape parameter, κ_0 the initial curvature, and $\theta(0)$ the initial heading. From (17), the path followed by a clothoid arc can be described by

$$x(\sigma) = A\int_0^\sigma \cos\theta(\tau)d\tau + x(0) \tag{18}$$

and

$$y(\sigma) = A\int_0^\sigma \sin\theta(\tau)d\tau + y(0) \tag{19}$$

where σ is the path variable evolving between 0 and 1, A is constant positive scaling factor, and $x(0)$ and $y(0)$ are the initial conditions of the arc.

We now wish to determine the different parameters of a clothoid arc (starting and ending points, shape factors). To do so, we will loosely follow the method from [1] (see also [4] for another reference on the use of clothoid arcs in robotics) and focus specifically on the first arc of Figure 5 (in red). As will be seen, the orientation of this particular arc will not result in a loss of generality, thanks to the structure of steering controller (15)-(16).

First, denote by α the angle between the two straight lines of the maneuver, intersecting at the origin (see Figure 5). Let the endpoint of the clothoid arc be situated at a distance b and an angle $\alpha/2$ from the origin. Then we have that

$$x(1) = b\cos\left(\pi - \frac{\alpha}{2}\right) \tag{20}$$

and

$$y(1) = b\sin\left(\pi - \frac{\alpha}{2}\right) \tag{21}$$

for the endpoint, while since the starting point is on the x-axis, we have $y(0) = 0$. Now referring to equation (17), it is clear from Figure 5 that $\kappa_0 = 0$ and $\theta(0) = 0$ on the first clothoid arc. Since $\theta(\sigma)$ is tangent to the path, we also have that

$$\theta(1) = -\frac{\pi + \alpha}{2} \tag{22}$$

which in turn leads to $k = 2\theta(1)$. It remains to determine $x(0)$ and A. Using (19) at $\sigma = 1$, we have

$$A = y(1)/\int_0^1 \sin(\theta(1)\tau^2)d\tau \tag{23}$$

Similarly, use (18) to obtain the starting point of the arc

$$x(0) = x(1) - A\int_0^1 \cos(\theta(1)\tau^2)d\tau \tag{24}$$

The other clothoid arc is simply obtained by symmetry. The first straight line segment can be simply computed with another parametrized curve

$$x(\sigma) = A\int_0^\sigma d\tau + x(0) \tag{25}$$

meaning this time that scale factor $A = x(1) - x(0)$, i.e. the distance between the two end points of the segment.The other straight line is also deduced by symmetry.

Note that because of the structure of controller (15)-(16) it is essentially parameters A and k that matter for each segment. Indeed, considering a straight line with an orientation θ_c, this would give

$$\frac{dx}{d\sigma}(\sigma) = A\cos\theta_c \tag{26}$$

and

$$\frac{dy}{d\sigma}(\sigma) = A\sin\theta_c \tag{27}$$

while, for a clothoid segment, we would have

$$\frac{dx}{d\sigma}(\sigma) = A\cos\theta(\sigma) \tag{28}$$

and

$$\frac{dy}{d\sigma}(\sigma) = A\sin\theta(\sigma) \tag{29}$$

Similarly, on a straight line, we would have

$$\frac{d\theta}{d\sigma}(\sigma) = 0 \tag{30}$$

while for a clothoid,

$$\frac{d\psi}{d\sigma}(\sigma) = k\sigma \tag{31}$$

Thus, taking into account (26)-(31) and regarding this time σ as a continuous parametrization on $[0, 4]$ for all segments, with each segment corresponding to a unit interval for σ, the steering controller equations are now

$$\dot{\sigma}(t) = \frac{v(t)}{A(\sigma(t))} \tag{32}$$

and

$$\delta(t) = \arctan\left(\frac{L}{A(\sigma(t))}\frac{d\theta}{d\sigma}(\sigma(t))\right) \tag{33}$$

where the scale factor $A(\sigma)$ changes on each segment.

The general aspect of the tacking maneuver path seems to be decided upon the value of the parameter b, which we recall, quantifies the distance between the outer point of the maneuver, and the intersection of the straight line segments. Thus, and as hinted at in the previous section, whether or not it is possible to cross the no-go zone while tacking could be linked with the choice of parameter b. To see this, first note that because of the straight line segments have their orientation *outside* the no-go zone, entering it will happen while the vehicle is on the first clothoid arc. Assuming the tacking maneuver starts from an angle $\theta(t) \leq -\theta_L$, and noting by θ_0 and θ_1 the start and end points of the arc, we have

$$\theta(\sigma) = (\theta_1 - \theta_0)\sigma^2 + \theta_0 \tag{34}$$

and the place on the curve where the vehicle enters the no-go zone corresponds to finding the value of σ, in (34), for which $\theta(\sigma) = -\theta_L$. Let us note this value σ_{-L}.

Similarly, leaving the no-sailing zone will happen on the second clothoid arc (still referring to θ_0 and θ_1 as the endpoints of the arc)

$$\theta(\sigma) = 3(\theta_1 - \theta_0)\sigma^2 + \frac{2}{3}(\theta_1 - \theta_0)\sigma + \theta_0 \tag{35}$$

and the value σ_L is obtained by solving $\theta(\sigma) = \theta_L$.

Values σ_{-L} and σ_L are then used to compute the length of the path in the no-go zone. Indeed, from (18) and (19) the length of each clothoid arc is A. From there, the length of the part of the first clothoid lying in the no-go zone is $A(1-\sigma_{-L})$, while for the second one, it is $A\sigma_L$, which finally gives us $A(1 - \sigma_{-L} + \sigma_L)$ for the length of the tacking path in the no-sailing zone. Since, from (10), l_∞ is the maximum distance that the vehicle can travel without propulsion, this implies the condition

$$A(1 - \sigma_{-L} + \sigma_L) < l_\infty \tag{36}$$

Note, from equation (23) that A depends on $y(1)$ which depends on b from (21). Hence, condition (36) transforms into

$$b < \frac{l_\infty}{k_\alpha(1 - \sigma_{-L} + \sigma_L)} \tag{37}$$

where

$$k_\alpha = \frac{\cos\left(\pi - \frac{\alpha}{2}\right)}{\int_0^1 \sin(\theta_1 \tau^2) d\tau} \tag{38}$$

From the point-of-view of motion planning, b can thus be tuned to satisfy (37). Note that l_∞ has to be computed from (10) first. Since the velocity of the vehicle before leaving the no-go zone, i.e. before v_0, is lesser or equal to v_0, we can choose to compute l_∞ from a point situated *before* the first clothoid arc. Condition (37) becomes a bit more conservative, but can be used directly for on-line motion planning.

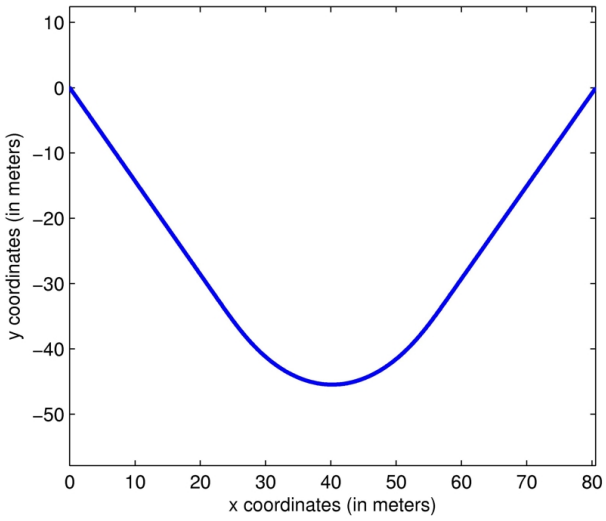

Fig. 6. Trajectory followed by the sailing vehicle.

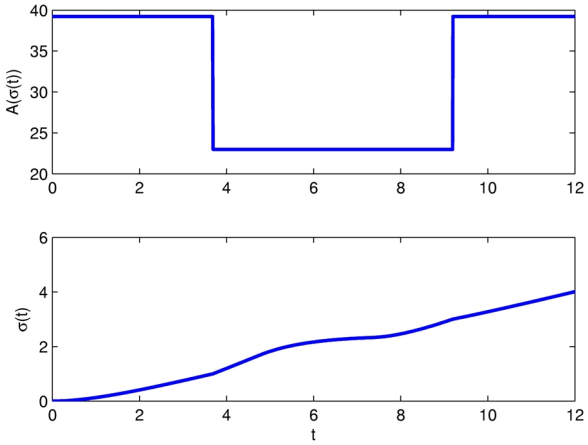

Fig. 7. Parameter $\sigma(t)$ and scale factor $A(\sigma(t))$.

To illustrate the behavior of dynamic controller (32)-(33), and of the role played by parameter b and its associated condition (37), we present a few simulation results with the vehicle parameters $m = 150$, $d = 135$ and $L = 2$. Maximum velocity $v_{\max}$ is set to 15. The sailing vehicle starts at a position $(0, 0)$ and performs a tacking maneuver, with a wind coming from the East, to go to position $(80, 0)$. The trajectory followed by the vehicle, with b satisfying condition (37) (in this simulation, we have $b = 12$), is shown in Figure 6. Figure 7 shows the evolution of path variable $\sigma(t)$ on the interval $[0, 4]$, switching from one segment of the maneuver to the next as $\sigma(t)$ reaches the next unit interval. This can also be seen from the upper plot of Figure 7, where scalar factor $A(\sigma)$ is represented.

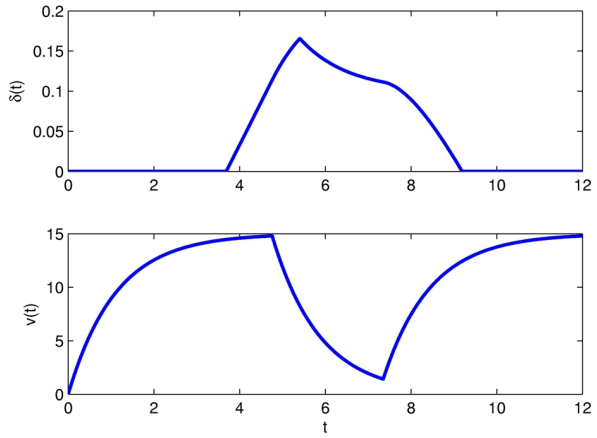

Fig. 8. Velocity $v(t)$ and steering angle $\delta(t)$.

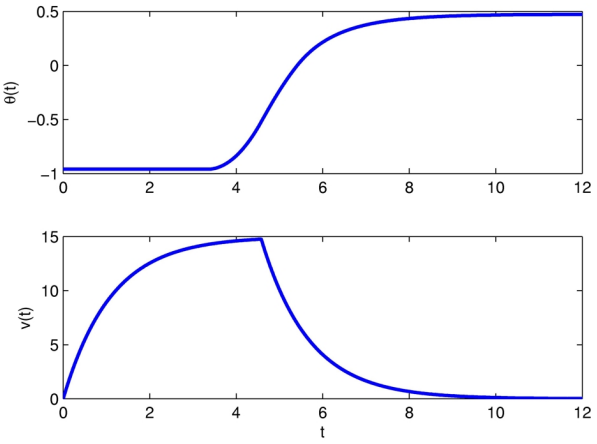

Fig. 9. Vehicle in irons

The evolution of the vehicle longitudinal velocity $v(t)$ is shown in the lower part of Figure 8. Note the decreasing values (after $t = 4s$) of $v(t)$ as the vehicle enters the no-sailing zone, then the re-acceleration as it escapes from it (before $t = 8s$). The corresponding steering angle, as obtained from controller (32)-(33) is shown in the upper part of the same figure.

Figure 9 shows another simulation illustrating a case when condition (37) is not fulfilled, and the initial velocity of the vehicle is not sufficient to allow it to cross the no-go zone (in this case, we had $b = 14$). The upper plot shows the angle of the vehicle trying to go to the limit $\theta_L = \pi/6$ of the no-go zone but never really reaching it ($\pi/6 \approx 0.5236$), while the lower plot shows the velocity decreasing continuously until it reaches zero, indicating that the vehicle is stuck in the no-go zone.

IV. Concluding remarks

This paper reported on a study of nonlinear aspects for trajectory and reference input generation for sailing vessels. The proposed model both represents in a simple way dynamics that are common to a wide variety of surface sailing vessels (landyachts, but also sailing boats, and systems with kites), and is also related to car-like robots that are widely studied in the mobile robotics community. The essence of the dynamics of sailing vessels seem to lie in the connection between the non-holonomic constraints of the vehicle together with the no-go zone, well-known to sailors, and is at the origin of the need for tacking maneuvers to go upwind. We proposed a simple way to describe paths associated with such maneuvers, and presented a simple controller to steer the vehicle on this path. A condition on the parametrization of the path for avoiding the vehicle to get stuck in the no-go zone was also introduced.

Other maneuvers such as wearing or boxhauling have also been done for centuries in sailing vessels [3]. Further work will examine motion planning for such cases, as well as design guidance systems combining such maneuvers.

References

[1] S. Fleury, P. Soueres, J.-P. Laumond and R. Chatila, "Primitives for smoothing mobile robot trajectories," *IEEE Transactions on Robotics and Automation*, vol. 11, no. 3, pp. 441–448, 1995.

[2] T. I. Fossen, *Marine control systems: guidance, navigation and control of ships, rigs and underwater vehicles*. Marine Cybernetics, 2002.

[3] J. Harland, *Seamanship in the age of sail*. Naval Institute Press, 1984.

[4] Y. Kanayama and B. I. Hartman, "Smooth local path planning for autonomous vehicles" in *Proc. IEEE Int. Conf. on Robotics and Automation*, Scottsdale, AZ, 1989.

[5] U. Kiencke and L. Nielsen, *Automotive Control Systems*. Springer, 2000.

[6] J.-P. Laumond (Ed.), *Robot motion planning and control*. Springer, 1998.

[7] S. M. LaValle, *Planning algorithms*. Cambridge University Press, 2006.

[8] C. A. Marchaj, *Aero-hydrodynamics of sailing*. International Marine Publishing, 1990.

[9] R. M. Murray and S. S. Sastry, "Nonholonomic motion planning: steering using sinusoids," *IEEE Transactions on Automatic Control*, vol. 38, no. 5, pp. 700–716, 1993.

[10] P. J. Richard, A. Johnson and A. Stanton, "America's cup downwind sails–vertical wings or horizontal parachutes?," *Journal of Wind Engineering and Industrial Aerodynamics*, vol. 89, pp. 1565–1577, 2001.

[11] E. D. Sontag, *Mathematical control theory (2nd ed.)*. Springer, 1998.

[12] C. M. Xiao and P. C. Austin, "Yacht modelling and adaptive control" in *Proc. IFAC Conf. on Manoeuvering and Control of Marine Craft*, Aalborg, Denmark, 2000.

[13] E. C. Yeh and J.-C. Bin, "Fuzzy control for self-steering of a sailboat" in *Proc. of the Singapore Int. Conf. on Intelligent Control and Instrumentation*, Singapore, 1992.